Comparison of functional connectivity between empirical and randomized structural brain networks

Seyma Bayrak, Philipp Hövel, Vesna Vuksanovic

This study combines experimental and modeling approaches in order to investigate the temporal dynamics of the human brain at rest. The dynamics of the neuronal activity is modeled with FitzHugh-Nagumo oscillators and the blood-oxygen-level-dependent (BOLD) time series is inferred via the Balloon-Windkessel hemodynamic model. The simulations are based on structural connections that are derived from diffusion-weighted magnetic resonance imaging measurements yielding anatomical probabilities between the considered brain regions of interest. In addition, the length of the fiber tracks allows for inference of coupling delays due to finite signal propagation velocities. We aim (i) to investigate the network topology of our neuroimaging data and (ii) how randomization of structural connections influence dynamics on top of it. The network characteristics of the structural connectivity data are compared to density-matched Erdős-Rényi random graphs. Furthermore, the neuronal and BOLD activity are modeled on both real and random (Erdős-Rényi type) graphs. The simulated temporal dynamics on both graphs are compared statistically to capture whether the spatial organization of these network affects the modeled time series. Results supported that key topological network properties such as small-worldness of our neuroimaging data are distinguishable from random networks. Moreover, the simulated BOLD activity on real and random graphs are observed to be dissimilar. The difference of the modeled temporal dynamics on the brain and random graphs suggests that anatomical connections in the human brain together with dynamical self-organization are crucial for the temporal evolution of the resting-state activity.

Comparison of functional connectivity between empirical and randomized structural brain networks

Şeyma Bayrak[1,2], Philipp Hövel[3,4], and Vesna Vuksanović[3,4,5]

[1]Institute of Biology, Otto-von-Guericke-Universität Magdeburg, Leipziger Straße 44, 39120 Magdeburg, Germany
[2]Max-Planck Institute for Human Cognitive and Brain Sciences, Stephanstraße 1a, 04103 Leipzig, Germany
[3]Institut für Theoretische Physik, Technische Universität Berlin, Hardenbergstraße 36, 10623 Berlin, Germany
[4]Bernstein Center for Computational Neuroscience Berlin, Humboldt-Universität zu Berlin, Philippstraße 13, 10115 Berlin, Germany
[5]Aberdeen Biomedical Imaging Centre, University of Aberdeen, Lilian Sutton Building, Foresterhill, Aberdeen AB25 2ZD, United Kingdom

ABSTRACT

This study combines experimental and modeling approaches in order to investigate the temporal dynamics of the human brain at rest. The dynamics of the neuronal activity is modeled with FitzHugh-Nagumo oscillators and the blood-oxygen-level-dependent (BOLD) time series is inferred via the Balloon-Windkessel hemodynamic model. The simulations are based on structural connections that are derived from diffusion-weighted magnetic resonance imaging measurements yielding anatomical probabilities between the considered brain regions of interest. In addition, the length of the fiber tracks allows for inference of coupling delays due to finite signal propagation velocities. We aim (i) to investigate the network topology of our neuroimaging data and (ii) how randomization of structural connections influence dynamics on top of it. The network characteristics of the structural connectivity data are compared to density-matched Erdős-Rényi random graphs. Furthermore, the neuronal and BOLD activity are modeled on both real and random (Erdős-Rényi type) graphs. The simulated temporal dynamics on both graphs are compared statistically to capture whether the spatial organization of these network affects the modeled time series. Results supported that key topological network properties such as small-worldness of our neuroimaging data are distinguishable from random networks. Moreover, the simulated BOLD activity on real and random graphs are observed to be dissimilar. The difference of the modeled temporal dynamics on the brain and random graphs suggests that anatomical connections in the human brain together with dynamical self-organization are crucial for the temporal evolution of the resting-state activity.

Keywords: brain networks, functional and anatomical connectivity, hemodynamic model, resting state, time-delayed oscillations

INTRODUCTION

Large-scale functional brain connectivity maps are networks of brain regions based on functional interactions, i.e. co-activation between these regions (Biswal et al., 1995; Bressler and Menon, 2010; Damoiseaux et al., 2006). In a typical functional magnetic resonance imaging (fMRI) experiment, functional connections are obtained from brain regions, whose corresponding time series of blood-oxygen-level-dependent (BOLD) activity display significant correlations at low-frequencies (< 0.1 Hz). Well organized spatio-temporal low-frequency fluctuations have been reported in BOLD-fMRI signals of a mammalian brain at rest, i.e. in the absence of any stimulation-driven task (Biswal et al., 1995; Damoiseaux et al., 2006; Vincent et al., 2007). Despite important progress over the past few years, the way how functional connectivity arises from complex anatomical connectivity still remains poorly understood (Ghosh et al., 2008b; Deco et al., 2009; Cabral et al., 2012, 2014; Vuksanović and Hövel, 2014).

Existing models of resting-brain dynamics hypothesize that functional interactions result from a

1

¹³ complex interplay between intrinsic brain dynamics and underlying structural connections (Hagmann
¹⁴ et al., 2008; Ghosh et al., 2008b; Rubinov et al., 2009; Deco and Jirsa, 2012; Vuksanović and Hövel,
¹⁵ 2016a,b). Previously, the neuronal dynamics have been modeled as coupled nonlinear oscillators (Wiener,
¹⁶ 1961; Lopes da Silva et al., 1997; Nunez, 1998, 2000; Poil et al., 2008), Hopf oscillators (Jirsa and
¹⁷ McIntosh, 2007), Wilson-Cowan systems (Deco et al., 2009), FitzHugh-Nagumo systems (Ghosh et al.,
¹⁸ 2008b; Vuksanović and Hövel, 2016a), and Kuramoto oscillators (Breakspear et al., 2010; Vuksanović
¹⁹ and Hövel, 2014, 2016b). In particular, these models explore the range of conditions at which functional
²⁰ networks emerge from anatomical connections: the role of multiple time-scales in the formation of
²¹ functional connectivity networks (Honey et al., 2007), time delays in the signal propagation between the
²² network nodes as well as the system noise (Ghosh et al., 2008a,b), local network oscillations (Deco et al.,
²³ 2009; Cabral et al., 2011), and structural disconnection (Cabral et al., 2012).

²⁴ Graph theory offers statistical tools to identify network structures, such as clustering coefficient and
²⁵ small-worldness property (Watts and Strogatz, 1998; Newman, 2010). Moreover, it introduces analytical
²⁶ or numerical methods to build random graphs, which are often referenced to characterize real-world
²⁷ networks. Random networks have been considered extensively as models of real-world networks of
²⁸ various types, extensively in ecological systems (May, 1972), in epidemiology (May and Lloyd, 2001;
²⁹ Kretzschmar and Morris, 1996), in metabolic pathways (Fell and Wagner, 2000), in social networks
³⁰ (Newman et al., 2001), and in neuronal networks of human brain (Watts and Strogatz, 1998; Bullmore and
³¹ Sporns, 2009; Simpson et al., 2011). A well known construction of random networks dates back to the
³² study of Paul Erdős and Alfred Rényi in 1959 (Erdős and Rényi, 1959) and these density-matched Erdős-
³³ Rényi type random graphs are well established. Furthermore, scale-free randomization (Barabási and
³⁴ Albert, 1999) and degree-preserving rewiring method citepmaslov2002specificity have been employed in
³⁵ last two decades.

³⁶ Our investigation provides a deeper insight into the relation between functional and anatomical brain
³⁷ connectivity: How is the dynamical process of brain's functional connectivity shaped by its structural
³⁸ topology? The considered networks are constructed from (i) binarized anatomical connectivity (AC) maps
³⁹ and (ii) their corresponding randomized counterparts generated via the Erdős-Rényi method (Erdős and
⁴⁰ Rényi, 1959). The neuronal activity and the BOLD fluctuations are simulated on both empirical structural
⁴¹ and randomized network types using the FitzHugh-Nagumo (FHN) model as proposed in (Ghosh et al.,
⁴² 2008a,b; Vuksanović and Hövel, 2015) and the Balloon-Windkessel hemodynamic model (Friston et al.,
⁴³ 2000), respectively. As system parameters, we vary the network density and the strengths of the delayed
⁴⁴ coupling. The purpose of this study is to explore how the simulated temporal dynamics of brain networks
⁴⁵ differ from the dynamics based on their randomized versions.

⁴⁶ The rest of this paper is organized as follows: In Sec. Materials & Methods, we introduce the empirical
⁴⁷ data set of AC map, describe the construction scheme of brain graphs based on AC map and corresponding
⁴⁸ random graphs. The temporal dynamics of the network nodes emerge from the FHN model and the
⁴⁹ Balloon-Windkessel hemodynamic model for the neuronal dynamics and BOLD time series, respectively
⁵⁰ (FitzHugh, 1961; Friston et al., 2000). The section closes with a summary of the statistical approaches
⁵¹ used to compare the empirical and simulated data sets. In Sec. Results & Discussion, we compare
⁵² network characteristics of brain and random graphs. Then, we analyze the similarity between the modeled
⁵³ temporal dynamics on brain graphs and that on random networks. Finally, Sec. Conclusion summarizes
⁵⁴ the key findings.

MATERIALS & METHODS

The Brain Graph

⁵⁷ The AC map is taken from the original study of Iturria-Medina et al. (2008). It is obtained from
⁵⁸ diffusion-weighted magnetic resonance imaging (DW-MRI) measurements with graph-based tractography
⁵⁹ procedures out of 20 healthy subjects (Iturria-Medina et al., 2008). The obtained network is based on
⁶⁰ $N = 90$ cortical and sub-cortical regions (*nodes*) defined by automated anatomic labeling (AAL) method
⁶¹ (Tzourio-Mazoyer et al., 2002). Within the AAL template, the indexes $1, 2, \ldots, 45$ refer to the right
⁶² hemisphere and regions labeled $46, 47, \ldots, 90$ correspond to the left hemisphere (Table 1). The values in
⁶³ the AC matrix refer to the probability of two AAL regions being connected at least by a single nervous
⁶⁴ fiber, see Figure 1.

⁶⁵ The brain graphs considered in the present study are generated by binarizing the empirical AC map
⁶⁶ via thresholding, that is, we define a threshold value for the connection probability p of node pairs. Then,
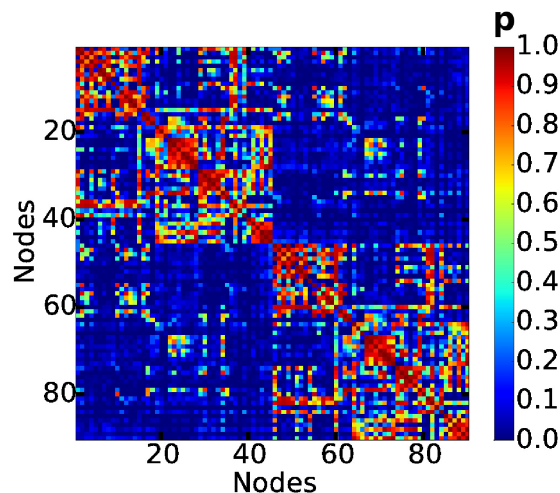
2/15

Figure 1. Empirical anatomical connectivity (AC) map of human cortex obtained from diffusion-weighted magnetic resonance imaging (DW-MRI) measurements (Iturria-Medina et al., 2008). The color bar shows probability of structural connections of node pairs in the AC map. Node index of the brain regions as in Table 1.

the values greater and equal to p are set to 1 in the connectivity matrix and to 0 otherwise. This way, the resulting binary *adjacency matrix* reflects the coupling topology of the brain graphs, which are treated as *undirected* and *unweighted* networks. In other words, all existing edges are thought to be of uniform weight and nodes interact both ways along an edge connecting them.

The Random Graph

In order to compare the effects of network structure of the brain graph with a generic network, we construct reference networks with the same *network density* κ in the form of random graphs. This follows a construction first discussed by Paul Erdős and Alfréd Rényi in their seminal paper (Erdős and Rényi, 1959). Given a total number of nodes N and total number of edges L, so-called Erdős-Rényi networks are undirected graphs $G(N,L)$, in which the presence of any edge between two nodes is realized with a fixed probability of $L/\binom{N}{2} = \frac{2L}{N(N-1)}$ (Newman, 2010). This results in a binomial distribution for the number of edges per node, known as the *degree*. A particular graph $G(N,L)$ is chosen uniformly random out of the set of all potential graphs having N nodes and L edges, which means the same *network density* κ.

In this study, we denote brain graphs as R_{BG} and Erdős-Rényi-type random graphs as R_{ER} for notational convenience. For an analysis of these graphs, we use the NETWORKX software package implemented in PYTHON (Hagberg et al., 2008).

Figure 2 illustrates an exemplary construction of adjacency matrices depicting the empirical connectivity map (panel A) as well as an Erdős-Rényi random graph (panel B). The brain graph is derived from the AC map seen in Figure 1 by applying a binarization threshold of $p = 0.54$.

The threshold range in this study is chosen to be in the $0.34 \leq p \leq 0.82$. The lower bound at $p = 0.34$ excludes extremely densely connected R_{BG}, i.e. almost all nodes connected to every other node. The upper limit is set to $p = 0.82$, when R_{BG} becomes disconnected.

FitzHugh-Nagumo Model for Neuronal Activity Simulations

The theoretical model of choice for the neuronal activity is the FitzHugh-Nagumo (FHN) system that phenomenologically describes physiological states of nerve membrane potential (FitzHugh, 1961; Nagumo et al., 1962). The FHN model is used to compute time series of neural activity i.e. activity of the neural populations placed in the regions of interest defined by AAL.

The local dynamics described by the FHN model consist of an activator variable x and an inhibitor variable y. Following the notation of Ghosh et al. (2008a,b), it is given by the following nonlinear
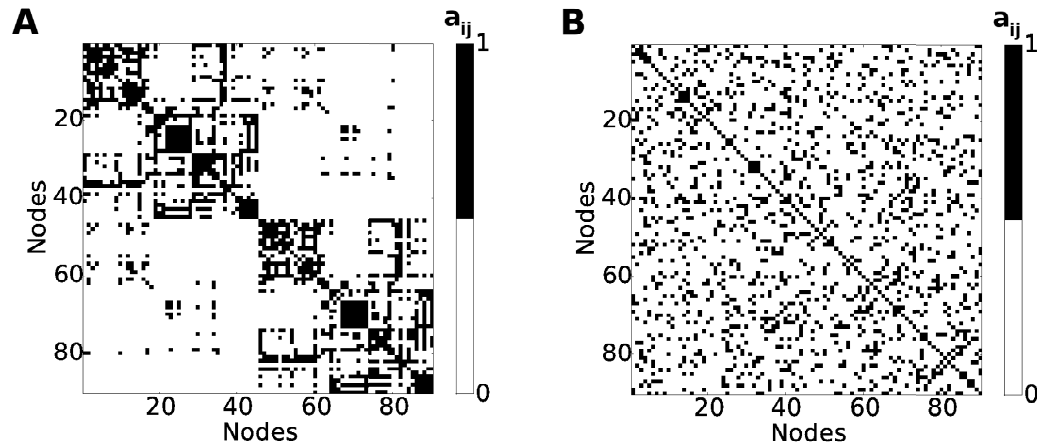
Figure 2. Construction of adjacency matrices: (A) The empirical AC map derived from DW-MRI data is binarized at a connection probability value $p = 0.54$. The black squares represent 1's indicating edges between nodes, whereas the white squares represent 0's implying no edge. The node index is chosen according to Table 1 (see Appendix). (B) An Erdős-Rényi random graph of the same network density.

differential equations:

$$\dot{x} = \tau\left(y + \gamma x - \frac{x^3}{3}\right) \tag{1a}$$

$$\dot{y} = -\frac{1}{\tau}(x - \alpha + \beta y), \tag{1b}$$

where τ denotes the time scale between the fast x- and slow y-variable, and γ, α, β are system parameters. x and y are considered to capture the dynamics of a neuronal population. The parameters in the FHN model are chosen such that solutions exhibit a damped oscillatory behavior for each node: $\alpha = 0.85$, $\beta = 0.2$, $\gamma = 1.0$, and $\tau = 1.25$ (Vuksanović and Hövel, 2016a). Thus, the fixed point of the system is a *stable focus*.

In order to simulate the neuronal activity, the FHN units are coupled as described by the following set of equations (Ghosh et al., 2008b; Vuksanović and Hövel, 2016a):

$$\dot{x}_i = \tau\left(y_i + \gamma x_i - \frac{x_i^3}{3}\right) - c\sum_{j=1}^{N} a_{ij}x_j\left(t - \Delta t_{ij}\right) + Dn_x \tag{2a}$$

$$\dot{y}_i = -\frac{1}{\tau}\left(x_i - \alpha + \beta y_i\right) + Dn_y, \tag{2b}$$

where indexes $i, j = 1, \ldots, N$ represent any node among the $N = 90$ AAL regions, c is the coupling strength, which scales the mutual time-delayed interactions, n_x, n_y represent Gaussian white noise sources with zero mean and unity variance and D is the noise strength. Here, $\{a_{ij}\}$ denotes the connectivity between nodes i and j in the adjacency matrix obtained from binarizing AC map at a specific connection probability (p) for the case of R_{BG}, or its randomized version for the case of R_{ER} (see Figure 2). If nodes are connected in a given network, then we have $a_{ij} = 1$, otherwise $a_{ij} = 0$. Δt_{ij} is the time delay taking into account a finite signal propagation velocity v between the nodes. Δt_{ij} is calculated as $\Delta t_{ij} = d_{ij}/v$ (Ghosh et al., 2008a,b; Deco et al., 2009), where d_{ij} is the approximated fiber length between nodes i and j (Iturria-Medina et al., 2008) as shown in Figure 3. We consider a biophysically realistic velocity of $v = 3$ m/s (Ghosh et al., 2008a). The noise strength is fixed at $D = 0.05$ throughout this study, which yields subthreshold oscillations. Thus, the system does not settle down to the fixed point.

The set of delay differential equations (2) is solved numerically using the PYTHON-module PYDE-LAY (*http://pydelay.sourceforge.net*) based on Bogacki-Shampine method (Bogacki and Shampine, 1989; Flunkert and Schöll, 2009). We simulate 7.5 minutes of neuronal activity, which corresponds to the length of the empirical BOLD measurement.
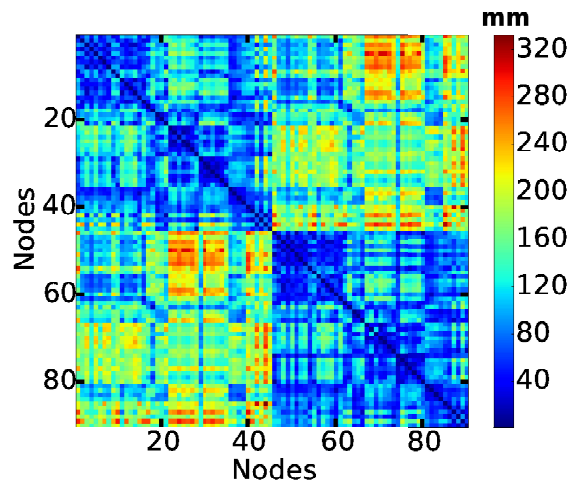
Figure 3. Distance matrix showing the approximated fiber lengths between node pairs d_{ij}(mm). Node index of the brain regions as in Table 1.

Balloon-Windkessel Model for BOLD Activity Simulations

From the simulated neuronal activity, we infer the BOLD signal observed in the fMRI data via the Balloon-Windkessel hemodynamic process (Friston et al., 2000). In short, the Balloon-Windkessel model uses the neuronal time series as an input signal (Seth et al., 2013) and computes hemodynamic oscillations analogous to the BOLD signal, which is modeled as a function of changes in cerebral blood flow, cerebral blood volume and cerebral metabolic rate of oxygen consumption. Most importantly, this model acts as a low-pass filter on the high-frequency neuronal input. The neuronal signal in the current study is the normalized time series of the activator variables of FHN model. We simulate 7.5 minutes of BOLD activity and discard transients of 20 s.

Comparing Brain Graphs to Random Graphs

The comparison of network measures between real-networks and random graphs have been already done in previous studies Bassett and Bullmore (2006); Humphries and Gurney (2008); Bullmore and Bassett (2011); Cabral et al. (2012), and our results are consistent with them (cf. Figure 4 and Appendix). In this study, we aim to compare the simulated functional connectivities (obtained from FHN network model and BOLD activity simulations) based on the brain graph R_{BG} and random graph R_{ER}. We quantify this comparison with Bhattacharya coefficients (Bhattacharyya, 1943), which is a statistical method broadly utilized in image processing (Goudail et al., 2004), speaker recognition (You et al., 2009) and phone clustering (Mak and Barnard, 1996).

Here, for all combinations of connectivity threshold p and coupling strength c, a functional connectivity matrix based on R_{BG} and R_{ER} is obtained for the modeled neuronal activity and BOLD activity. The connectivity matrices are calculated via the Pearson's correlation coefficient ρ_{ij},

$$\rho_{ij} = \frac{\langle u_i(t)u_j(t)\rangle - \langle u_i(t)\rangle\langle u_j(t)\rangle}{\sigma(u_i(t))\sigma(u_j(t))}, \tag{3}$$

where $u_i(t)$ denotes the modeled time series (simulated FHN or BOLD activity) of the node i, σ stands for standard deviation and $\langle \cdot \rangle$ represents the temporal average. This yields a 90×90 correlation matrix $\{\rho_{ij}\}$, which is referred to as simulated functional connectivity (FC$_s$).

Since the position of the nodes in the brain graph R_{BG} and its randomized versions R_{ER}, the Pearson's correlation method is not a good measure for comparison of the functional connectivity. To quantify the similarity of modeled temporal activity - FC$_s$ maps - on R_{BG} and R_{ER}, we calculate Bhattacharya coefficients instead. This follows a widely used statistical approach to measure the dissimilarity between histogram distributions (Bhattacharyya, 1943).

Let us denote the histogram of simulated correlation ρ_{ij}-values in FC$_s$ obtained from R_{BG} by H_{BG} and that from R_{ER} by H_{ER}. Then, the Bhattacharya coefficient $d(H_{BG}, H_{ER})$ is given by the following

equation:

$$d\left(H_{BG},H_{ER}\right) = \sqrt{1 - \frac{1}{\sqrt{\overline{H}_{BG}\,\overline{H}_{ER}N^2}}\sum_i \sqrt{H_{BG}(i)H_{ER}(i)}}, \tag{4}$$

where $\overline{H}$ denotes the mean of the histogram H (Bhattacharyya, 1943). $d\left(H_{BG},H_{ER}\right)$ is scaled between 0 and 1. A high $d\left(H_{BG},H_{ER}\right)$ value indicates a small overlap of H_{BG} and H_{ER}, whereas a low $d\left(H_{BG},H_{ER}\right)$ value expresses a high degree of similarity. For an exemplary histogram comparison with this method, see Figure 7 in Appendix.

RESULTS & DISCUSSION

The structural organization in the brain, the topology of anatomical-connectivity maps, affects the temporal evolution of the simulated neuronal activity and BOLD signal. Moreover, they were different from the modeled BOLD signals based on density-matched Erdős-Rényi type networks (Figure 5). Our findings suggested that only very weak coupling strengths result in similar distributions of functional correlations (Figure 6B). This would imply that low coupling strengths cannot effectively capture the time-delay effects of FitzHugh-Nagumo systems. However, it was possible to capture distinctive temporal dynamics between the real neuronal network and density-matched Erdős-Rényi type random graph over a wide range of parameters (Figure 5, Figure 6A). Therefore, the systematic hierarchical structure of human brain contributes to the evolution of its temporal dynamics at the resting-state.

The AC map was binarized at several connection probability values in the range of $0.34 \leq p \leq 0.82$. The resulting adjacency matrices at each p-value were further used to build the brain graphs R_{BG}. This way, the cortical and sub-cortical AAL regions were denoted as *nodes*, and the thresholded anatomical connectivity probabilities were represented by *edges* yielding unweighted networks. In order to investigate the hierarchical arrangement of the anatomy in the human brain, we compared the standard statistical network measures of R_{BG} to that of the randomized networks. Here, we manipulated the adjacency matrices via Erdős-Rényi-type randomization and constructed their corresponding graphs R_{ER}. In fact, several randomization procedures have been performed for this study, e.g. configuration model or partial randomization (see Appendix, Figure 8), but we decided to draw our conclusions based on density-matched Erdős-Rényi random graph comparisons, since they are well established and have often been studied previously (Erdős and Rényi, 1959; Bullmore and Bassett, 2011).

The standard topological properties of the brain graph R_{BG} and random graph R_{ER} are illustrated in Figure 4. Note that the network density κ, *average clustering coefficients C*, and *small-worldness S* of each network were calculated and visualized in dependence on the binarization threshold p. For formal definitions of C and S, see Appendix. Figure 4A shows that κ of R_{BG} is preserved in R_{ER}, as expected from the definition of Erdős-Rényi-type randomization. κ decreases sigmoidally with increasing p. Figure 4B indicates that the nodes in R_{BG} tend to cluster more more than in R_{ER}. Therefore, the local information transfer is expected to be more efficient in R_{BG}. Moreover, R_{BG} exhibits clearly small-world network characteristics with its highly clustered nodes and short characteristic pathways compared to R_{ER} (Figure 4C). In fact, the small-worldness measure S provides the clearest distinction between R_{BG} and R_{ER}, indicating that the real networks are both highly segregated and integrated (Humphries and Gurney, 2008). Here, the term segregation points to a specialized information processing, whereas integration refers to a distributed one (Bassett and Bullmore, 2006). Our findings concerning the hierarchy in the anatomical connectivity are in agreement with previous studies of Bassett and Bullmore (2006); Humphries and Gurney (2008); Bullmore and Bassett (2011) as well as the studies performed on cat and macaque monkey (Sporns and Zwi, 2004; Sporns et al., 2004). Furthermore, we extended the analysis of non-random topological characteristics of human anatomical connectivity into its temporal dynamical properties. Our aim was to investigate whether the modeled temporal activity of real neuronal networks would differ from that of density-matched Erdős-Rényi random graphs. For this purpose, we simulated both R_{BG} and R_{ER} with previously reviewed resting-state neuronal and BOLD activity models. Then, we statistically compared the simulated functional connectivity (FC_s) matrices based on R_{BG} and R_{ER}.

The neuronal activity of each node in R_{BG} and R_{ER} was simulated with the FitzHugh-Nagumo (FHN) network dynamics as given in equations (2a) and (2b), which drives nodes from their equilibrium state to oscillatory behavior because of the Gaussian white noise term and the coupling (Hövel, 2010). The FHN system has been studied in detail to analyze neuronal systems (Schöll et al., 2009; Hövel et al.,
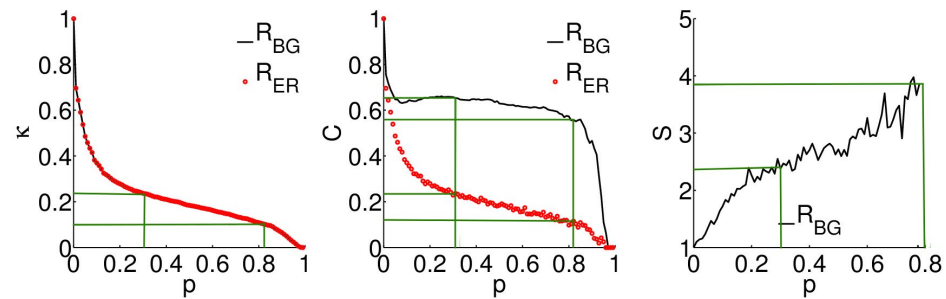
Figure 4. Statistical network characteristics of R_{BG} (black curves) and R_{ER} (red dots): (A) Network density κ, (B) cluster coefficient C and (C) small-worldness coefficient S. Note that the S-value is defined as a ratio of network measures of R_{BG} to R_{ER}, see Appendix. S is only shown in the range, where the network is connected. Green lines correspond to the network measures in the range of $0.34 \le p \le 0.82$.
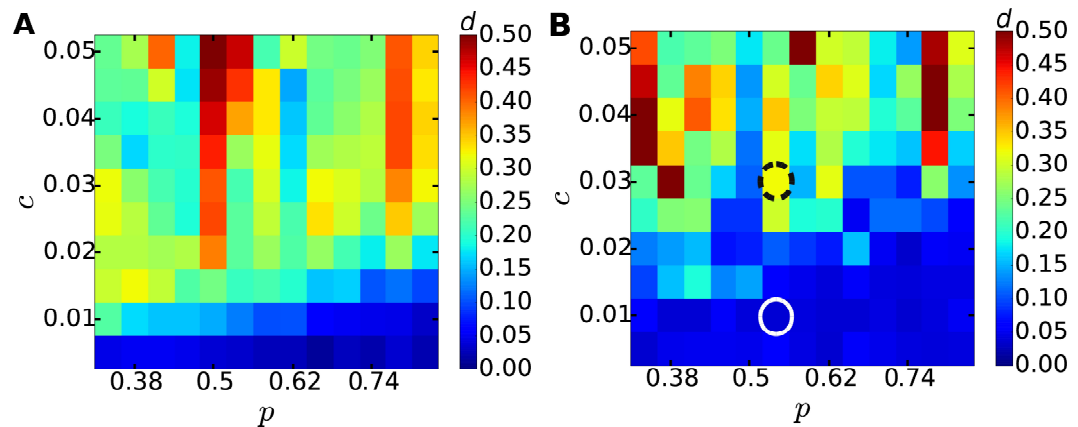

Figure 5. Statistical comparison of brain graphs R_{BG} and random graphs R_{ER} in terms of their modeled temporal dynamics: (A) FHN network model (parameters: $\alpha = 0.85$, $\beta = 0.2$, $\gamma = 1.0$, $\tau = 1.25$, and $v = 3$ m/s) and (B) modeled BOLD activity. The heat map represents the degree of similarity $d(H_{BG}, H_{ER})$ between histogram distributions of simulated functional connectivity of R_{BG} and R_{ER}. Large d (warm colors) represents low similarity, low d (cold colors) refers to high degree of similarity. Dashed circle ($p = 0.54$, $c = 0.03$) and solid circle ($p = 0.54$, $c = 0.01$) are chosen to display different and similar histogram distributions in Figure 6.

2010; Panchuk et al., 2013). Here, we used the notations of Ghosh et al. (2008a,b) and Vuksanović and Hövel (2016a), which were designed to capture the empirical resting-state FC by modeling the empirical AC map of non-human primate (macaque) and human, respectively. It was shown that the simulated FC obtained at weak coupling strengths c was in a high agreement with the empirical FC (Ghosh et al., 2008a,b; Vuksanović and Hövel, 2016a). In order to obtain biologically plausible temporal dynamics on our neuroimaging data, we restricted our c-values in a similar range that was justified physiologically. The modeled FHN time series were in high frequency ranges beyond 20 Hz. Therefore, a modulation of these neuronal time series was done by applying the standard Balloon-Windkessel hemodynamic model, which acted as a low-pass filter, and therefore resulted in ultra slow frequency below 0.1 Hz in the simulated BOLD time series (Friston et al., 2000).

At each (p, c)-value, an FC_s matrix was calculated via Pearson's correlation coefficients for the neuronal and BOLD activity simulations, separately. Figure 5 compares these simulated temporal dynamics on the brain graph R_{BG} and the random graph R_{ER} for the FHN network model and the Balloon-Windkessel model in panels (A) and (B), respectively. Since the topology of the nodes were not identical in R_{BG} and R_{ER}, the standard Pearson's correlation method was not used to compare their FC_s matrices. Instead, the comparisons were quantified using another statistical tool, namely Bhattacharya coefficients $d(H_{BG}, H_{ER})$ given by color bars, where H_{BG} and H_{ER} refer to the histogram of the FC_s matrices of
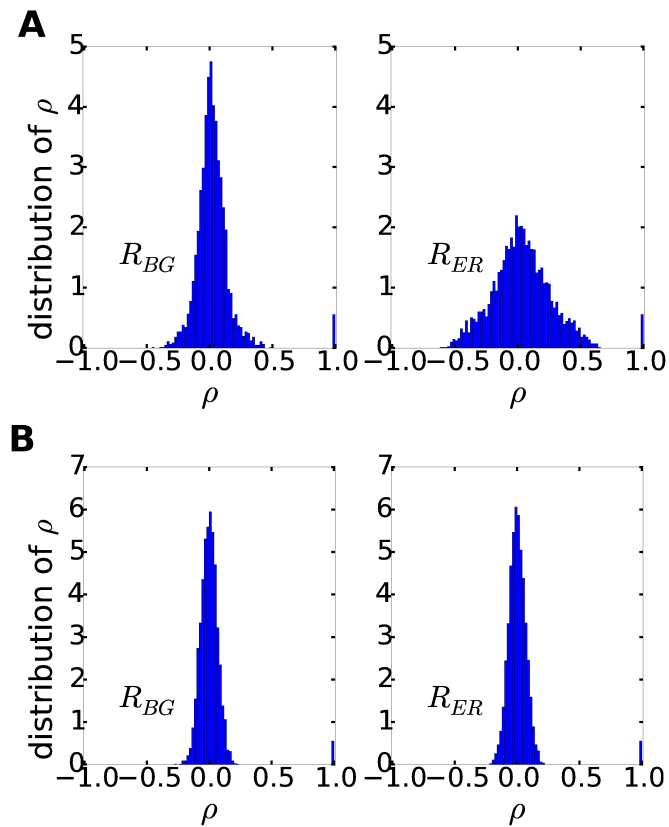
Figure 6. Two exemplary histograms chosen from red color from the cold color in Figure 5 exhibiting differences ($c = 0.03$, panel (A), see dashed circle in Figure 5) and similarity ($c = 0.01$, panel (B), see solid circle in Figure 5). Parameters as in Figure 5.

simulations on R_{BG} and R_{ER}, respectively.

In Figure 5, the hot colors indicated a difference between the distributions of ρ_{ij}-values, namely H_{BG} and H_{ER}, whereas the cold colors represented the similarity of the histograms. The FC_s based on the neuronal time series modeled by the FHN equations on network R_{BG} can be clearly distinguished from that of R_{ER}, Figure 5A. $d(H_{BG}, H_{ER})$ is small at very weak coupling strengths and thus, the histograms are similar. The nodes in the adjacency matrix of the AC map tend to have more connections intrahemispherically (see a_{ij}-values clustering for right-right and left-left combinations of nodal pairs in the top left and bottom right quadrant of the adjacency matrix depicted Figure 2A), implying that the fiber lengths d_{ij} taken into account for FHN network dynamics were mostly shorter (Figure 3). On the other hand, connections among nodes in R_{ER} were distributed more homogeneously (Figure 2B), and thus long d_{ij}-values were employed as often as short d_{ij}-values in the FHN network model. Therefore, the density-matched Erdős-Rényi random graph had much longer time-delays Δt_{ij} than R_{ER}. This effect causes a dissimilarity between our modeled neuronal dynamics on R_{BG} and R_{ER}. However, at low c-values, the effect of time-delays vanishes.

Figure 6 illustrated exemplary histograms based on the simulated BOLD time series for R_{BG}, which were constructed on an adjacency matrix obtained at $p = 0.54$, and for a corresponding random graph R_{ER}. The distribution of ρ_{ij}-values in R_{BG} and R_{ER} was single-peaked and almost symmetric to zero for $c = 0.03$ (panel A) and $c = 0.01$ (panel B). The peaks at $\rho = 1.0$ in each graph corresponded to self-paired nodes, i.e. $\rho_{ij} = 1.0$. However, for $c = 0.03$ the distribution in R_{ER} was broader than for R_{BG}, that was, the presence of both correlated and anti-correlated node pairs is more dominant for R_{ER}. In contrast, the distributions became very similar and narrow for $c = 0.01$, there are mostly no correlations among the modeled BOLD signals in both network types (panel B).

Cabral et al. (2012) previously studied effects of a pathological disconnection, i.e. potentially leading to schizophrenia, by randomly pruning anatomical connections, that means, the links in the

original anatomical network were removed randomly by changing connection strengths of nodes. Their [230] results demonstrated that disconnected anatomical networks have lower small-worldness and clustering [231] coefficients and moreover, the structural disconnection causes dramatical alterations in their corresponding [232] simulated functional networks (Cabral et al., 2012). In our study, we disputed the AC map by rewiring [233] the links while keeping the network density fixed. Despite of different randomization techniques, i.e. [234] rewiring versus removing edges, our study illustrates similar findings with Cabral et al. (2012): The [235] functional connectivity in brain emerges mainly through the interplay between the long distance brain [236] connectivity and the local dynamics. The dominant long-range intra-hemispheric connections in the [237] original AC map was lost in the Erdős-Rényi type random networks, and the local dynamical properties [238] such as clustering coefficient of nodes decreased gradually in R_{ER}. The loss of hierarchy in the anatomical [239] structure provokes a discriminative FC_s. However, when the coupling strengths in the modeled temporal [240] dynamics are too weak, then the FC_s based on both the R_{BG} and R_{ER} tends to be random (Figure 6B). [241]

CONCLUSION [242]

In this study, we have simulated resting-state functional connectivity in the human brain based on [243] empirically derived structural networks and their randomized topologies. Our aim was to explore the [244] network topology of our anatomical neuroimaging data and moreover to investigate how the temporal [245] dynamics modeled on brain networks differs from the dynamics on random networks. We have addressed [246] the topological characteristics of brain graphs, which were built on structural connectivity data, as [247] well as density-matched Erdős-Rényi type random graphs. Moreover, the difference between brain [248] and randomized brain structural connectivity has been analyzed by comparing their modeled temporal [249] dynamics; the FHN network model for the neuronal activity and the Balloon-Windkessel model for the [250] BOLD activity. We have demonstrated that the simulated neuronal time series of brain graphs are clearly [251] distinguishable from that of random networks at relatively low coupling strengths and at the network [252] density range of $0.14 \leq \kappa \leq 0.22$. This holds additionally for the simulated BOLD signal diversity [253] between two network types. [254]

ACKNOWLEDGMENTS [255]

REFERENCES [259]

Barabási, A.-L. and Albert, R. (1999). Emergence of scaling in random networks. *science*, 286(5439):509– [260] 512. [261]

Bassett, D. and Bullmore, E. (2006). Small-world brain networks. *The Neuroscientist*, 12(6):512–523. [262]

Bhattacharyya, A. (1943). On a measure of divergence between two statistical populations defined by [263] their probability distributions. *Bulletin of the Calcutta Mathematical Society*, 35:99–109. [264]

Biswal, B., Yetkin, F. Z., Haughton, V. M., and Hyde, J. S. (1995). Functional connectivity in the [265] motor cortex of resting human brain using echo-planar MRI. *Magnetic Resonance in Medicine*, [266] 34(4):537–541. [267]

Bogacki, P. and Shampine, L. F. (1989). A 3(2) pair of runge - kutta formulas. *Applied Mathematics* [268] *Letters*, 2(4):321–325. [269]

Breakspear, M., Heitmann, S., and Daffertshofer, A. (2010). Generative models of cortical oscillations: [270] neurobiological implications of the kuramoto model. *Frontiers in human neuroscience*, 4(190):1–14. [271]

Bressler, S. L. and Menon, V. (2010). Large-scale brain networks in cognition: emerging methods and [272] principles. *Trends in Cognitive Sciences*, 14(6):277–290. [273]

Bullmore, E. T. and Bassett, D. S. (2011). Brain graphs: graphical models of the human brain connectome. [274] *Annual review of clinical psychology*, 7:113–140. [275]

Bullmore, E. T. and Sporns, O. (2009). Complex brain networks: graph theoretical analysis of structural [276] and functional systems. *Nat. Rev. Neurosci.*, 10(3):186–198. [277]

Cabral, J., Hugues, E., Kringelbach, M. L., and Deco, G. (2012). Modeling the outcome of structural [278] disconnection on resting-state functional connectivity. *NeuroImage*, 62:1342–1353. [279]

280 Cabral, J., Hugues, E., Sporns, O., and Deco, G. (2011). Role of local network oscillations in resting-state
281 functional connectivity. *NeuroImage*, 57(1):130–139.

282 Cabral, J., Kringelbach, M. L., and Deco, G. (2014). Exploring the network dynamics underlying brain
283 activity during rest. *Progress in Neurobiology*, 114:102–131.

284 Damoiseaux, J. S., Rombouts, S. A. R. B., Barkhof, F., Scheltens, P., Stam, C. J., Smith, S. M., and
285 Beckmann, C. F. (2006). Consistent resting-state networks across healthy subjects. *Proc. Natl. Acad.
286 Sci. U.S.A.*, 103(37):13848–13853.

287 Deco, G. and Jirsa, V. K. (2012). Ongoing cortical activity at rest: criticality, multistability, and ghost
288 attractors. *The Journal of Neuroscience*, 32(10):3366–3375.

289 Deco, G., Jirsa, V. K., McIntosh, A. R., Sporns, O., and Kötter, R. (2009). Key role of coupling, delay,
290 and noise in resting brain fluctuations. *Proc. Natl. Acad. Sci. U.S.A.*, 106(25):10302–10307.

291 Erdős, P. and Rényi, A. (1959). On random graphs. i. *Publicationes Mathematicae*, 6:290–297.

292 Fell, D. A. and Wagner, A. (2000). The small world of metabolism. *Nature biotechnology*, 18(11):1121–
293 1122.

294 FitzHugh, R. (1961). Impulses and physiological states in theoretical models of nerve membrane. *Biophys.
295 J.*, 1:445–466.

296 Flunkert, V. and Schöll, E. (2009). pydelay – a python tool for solving delay differential equations.
297 arXiv:0911.1633 [nlin.CD].

298 Friston, K., Mechelli, A., Turner, R., and Price, C. J. (2000). Nonlinear responses in fMRI: The balloon
299 model, Volterra kernels, and other hemodynamics. *NeuroImage*, 12(4):466–477.

300 Ghosh, A., Rho, Y., McIntosh, A. R., Kötter, R., and Jirsa, V. K. (2008a). Cortical network dynamics with
301 time delays reveals functional connectivity in the resting brain. *Cogn. Neurodyn.*, 2(2):115–120.

302 Ghosh, A., Rho, Y., McIntosh, A. R., Kötter, R., and Jirsa, V. K. (2008b). Noise during rest enables the
303 exploration of the brain's dynamic repertoire. *PLoS Comput Biol*, 4(10):e1000196.

304 Goudail, F., Réfrégier, P., and Delyon, G. (2004). Bhattacharyya distance as a contrast parameter for
305 statistical processing of noisy optical images. *JOSA A*, 21(7):1231–1240.

306 Hagberg, A. A., Schult, D. A., and Swart, P. J. (2008). Exploring network structure, dynamics, and
307 function using NetworkX. *Proceedings of the 7th Python in Science Conference (SciPy2008)*, pages
308 11–15.

309 Hagmann, P., Cammoun, L., Gigandet, X., Meuli, R., Honey, C., Wedeen, V., and Sporns, O. (2008).
310 Mapping the structural core of human cerebral cortex. *PLoS Biology*, 6(7):15.

311 Honey, C. J., Kötter, R., Breakspear, M., and Sporns, O. (2007). Network structure of cerebral cortex
312 shapes functional connectivity on multiple time scales. *Proc. Natl. Acad. Sci. U.S.A.*, 104:10240–10245.

313 Hövel, P. (2010). *Control of complex nonlinear systems with delay*. Springer Science & Business Media.

314 Hövel, P., Dahlem, M. A., and Schöll, E. (2010). Control of synchronization in coupled neural systems by
315 time-delayed feedback. *International Journal of Bifurcation and Chaos*, 20(03):813–825.

316 Humphries, M. D. and Gurney, K. (2008). Network 'small-world-ness' : a quantitative method for
317 determining canonical network equivalence. *PLoS One*, 3(4):e0002051.

318 Iturria-Medina, Y., Sotero, R. C., Canales-Rodríguez, E. J., Alemán-Gómez, Y., and Melie-García, L.
319 (2008). Studying the human brain anatomical network via diffusion-weighted MRI and graph theory.
320 *Neuroimage*, 40(3):1064–1076.

321 Jirsa, V. K. and McIntosh, A. R. (2007). *Handbook of brain connectivity*. Springer.

322 Kretzschmar, M. and Morris, M. (1996). Measures of concurrency in networks and the spread of infectious
323 disease. *Mathematical biosciences*, 133(2):165–195.

324 Latora, V. and Marchiori, M. (2001). Efficient behavior of small-world networks. *Phys. Rev. Lett.*,
325 87(19):198701.

326 Lopes da Silva, F., Pijn, J., Velis, D., and Nijssen, P. (1997). Alpha rhythms: noise, dynamics and models.
327 *International Journal of Psychophysiology*, 26(1-3):237–249.

328 Mak, B. and Barnard, E. (1996). Phone clustering using the bhattacharyya distance. In *Spoken Language,
329 1996. ICSLP 96. Proceedings., Fourth International Conference on*, volume 4, pages 2005–2008. IEEE.

330 Maslov, S. and Sneppen, K. (2002). Specificity and stability in topology of protein networks. *Science*,
331 296(5569):910–913.

332 May, R. M. (1972). Will a large complex system be stable? *Nature*, 238:413–414.

333 May, R. M. and Lloyd, A. L. (2001). Infection dynamics on scale-free networks. *Physical Review E*,
334 64(6):066112.

Nagumo, J., Arimoto, S., and Yoshizawa., S. (1962). An active pulse transmission line simulating nerve axon. *Proc. IRE*, 50:2061–2070.

Newman, M. E., Strogatz, S. H., and Watts, D. J. (2001). Random graphs with arbitrary degree distributions and their applications. *Physical review E*, 64(2):026118.

Newman, M. E. J. (2003). The structure and function of complex networks. *SIAM Review*, 45(2):167–256.

Newman, M. E. J. (2010). *Networks: an introduction*. Oxford University Press, Inc., New York.

Nunez, P. L. (1998). *Electric fields of the brain: the neurophysics of EEG*. New York: Oxford university press.

Nunez, P. L. (2000). Toward a quantitative description of large-scale neocortical dynamic function and eeg. *Behavioral and Brain Sciences*, 23(03):371–398.

Panchuk, A., Rosin, D. P., Hövel, P., and Schöll, E. (2013). Synchronization of coupled neural oscillators with heterogeneous delays. *International Journal of Bifurcation and Chaos*, 23(12):1330039.

Poil, S.-S., van Ooyen, A., and Linkenkaer-Hansen, K. (2008). Avalanche dynamics of human brain oscillations: relation to critical branching processes and temporal correlations. *Human brain mapping*, 29(7):770–777.

Rubinov, M. and Sporns, O. (2010). Complex network measures of brain connectivity: uses and interpretations. *NeuroImage*, 52(3):1059–1069.

Rubinov, M., Sporns, O., van Leeuwen, C., and Breakspear, M. (2009). Symbiotic relationship between brain structure and dynamics. *BMC Neuroscience*, 10(1):55.

Schöll, E., Hiller, G., Hövel, P., and Dahlem, M. A. (2009). Time-delayed feedback in neurosystems. *Philosophical Transactions of the Royal Society of London A: Mathematical, Physical and Engineering Sciences*, 367(1891):1079–1096.

Seth, A. K., Chorley, P., and Barnett, L. C. (2013). Granger causality analysis of fmri bold signals is invariant to hemodynamic convolution but not downsampling. *Neuroimage*, 65:540–555.

Simpson, S. L., Hayasaka, S., and Laurienti, P. J. (2011). Exponential random graph modeling for complex brain networks. *PLoS One*, 6(5):e20039.

Sporns, O., Chialvo, D. R., Kaiser, M., and Hilgetag, C. C. (2004). Organization, development and function of complex brain networks. *Trends in cognitive sciences*, 8(9):418–425.

Sporns, O. and Zwi, J. D. (2004). The small world of the cerebral cortex. *Neuroinformatics*, 2(2):145–162.

Tzourio-Mazoyer, N., Landeau, B., Papathanassiou, D., Crivello, F., Etard, O., Delcroix, N., Mazoyer, B., and Joliot, M. (2002). Automated anatomical labeling of activations in SPM using a macroscopic anatomical parcellation of the MNI MRI single-subject brain. *Neuroimage*, 15(1):273–289.

Vincent, J. L., Patel, G. H., Fox, M. D., Snyder, A. Z., Baker, J. T., van Essen, D. C., Zempel, J. M., Snyder, L. H., Corbetta, M., and Raichle, M. E. (2007). Intrinsic functional architecture in the anaesthetized monkey brain. *Nature*, 447(7140):83–86.

Vuksanović, V. and Hövel, P. (2014a). Functional connectivity of distant cortical regions: Role of remote synchronization and symmetry in interactions. *NeuroImage*, 97:1–8.

Vuksanović, V. and Hövel, P. (2015). Dynamic changes in network synchrony reveal resting-state functional networks. *Chaos: An Interdisciplinary Journal of Nonlinear Science*, 25(2):023116.

Vuksanović, V. and Hövel, P. (2016). Large-scale neural network model for functional networks of the human cortex. In Pelster, A. and Wunner, G., editors, *Selforganization in Complex Systems: The Past, Present, and Future of Synergetics, Proc. of the International Symposium, Hanse Institute of Advanced Studies Delmenhorst*, Berlin. Springer, 345–352.

Vuksanović, V. and Hövel, P. (2016). Role of structural inhomogeneities in resting-state brain dynamics. *Cognitive Neurodynamics* in print.

Watts, D. J. and Strogatz, S. H. (1998). Collective dynamics of 'small-world' networks. *Nature*, 393:440–442.

Wiener, N. (1961). *Cybernetics: Or, Control and Communication in the Animal and the Machine*. Cambridge (Massachussetts): MIT press.

You, C. H., Lee, K. A., and Li, H. (2009). An svm kernel with gmm-supervector based on the bhattacharyya distance for speaker recognition. *Signal Processing Letters, IEEE*, 16(1):49–52.

APPENDIX

Network Characterizations

A network can be statistically described in terms of its topology, i.e. solely in terms of its connectivity and independently of spatial positions of nodes and edges. In this work, it is aimed to characterize the topology of the brain graph R_{BG} and its randomized versions R_{ER}.

Network Density The *average degree* $\langle k \rangle$ of a network is proportional to the ratio of total number of edges L to total number of nodes N in a graph,

$$\langle k \rangle = \frac{2L}{N}. \tag{5}$$

The *density* κ of a network is formulated as the ratio between L and maximum number of possible edges $\binom{N}{2}$,

$$\kappa = \frac{2L}{N(N-1)}. \tag{6}$$

The measure of network density can be referred to as the total *wiring cost* of the network (Rubinov and Sporns, 2010). The *degree* of an individual node k_i, average degree $\langle k \rangle$ and network density κ are key scalar measures to characterize the topology of a network.

Average Clustering Coefficient The *average clustering coefficient C* of a network is calculated through individual clustering coefficients C_i of single nodes,

$$C = \frac{1}{n} \sum_{i \varepsilon N} C_i = \frac{1}{n} \sum_{i \varepsilon N} \frac{2t_i}{k_i(k_i - 1)}, \tag{7}$$

where t_i is the number of triangles around node i (Watts and Strogatz, 1998). The clustering coefficient C_i of a node i is a measure of local connectivity and is highly correlated with the local efficiency of the information transfer (Latora and Marchiori, 2001). The average clustering coefficient C is a normalized version of C_i for the whole network, yielding now a global property. C is a measure of segregation, that is, the ability for specialized processing to occur within densely interconnected groups of brain regions (Rubinov and Sporns, 2010). It reveals how the individual nodes in a graph cluster together; how many neighbors of a node are neighbors of each other.

Small-Worldness A small world network is both highly segregated and integrated, a measure of small worldness S was proposed to capture this effect in a single statistic,

$$S = \frac{C/C_{rand}}{l/l_{rand}} \qquad \text{with} \qquad l = \frac{1}{n} \sum_{i \varepsilon N} l_i = \frac{1}{n} \sum_{i \varepsilon N} \frac{\sum\limits_{j \varepsilon N, j \neq i} s_{ij}}{n-1}, \tag{8}$$

where C and C_{rand} are clustering coefficients, l and l_{rand} are characteristic path lengths of the original and random network respectively (Humphries and Gurney, 2008). The random network here is constructed with *Erdős-Rényi* method, which has the same number of nodes and links as the reference graph. l is calculated through the shortest path length s_{ij} between nodes i and j, a basis for measuring integration (Rubinov and Sporns, 2010).

Bhattacharya Coefficient

Figure 7A represents the histogram of a Gaussian distribution H_A, the dashed red curve is its probability density function with mean $\mu = 15$ and standard deviation $\sigma = 1.0$. Figure 7B displays the histogram distribution of a Gaussian mixture in a bimodal shape H_B, the red dashed curve is its Kernel density estimation, the peaks are centered at $\mu_l = 11$ and $\mu_r = 19$. The Bhattacharya coefficient between H_A and H_B is found to be $d(H_A, H_B) = 0.63$, indicating that two distributions are dissimilar. However, once H_A is compared with itself, then $d(H_A, H_A) = 0.03$ indicating an analogy. Note that there still remains a small, finite value $d(H_A, H_A) \neq 0$, since the values chosen to be random distributions fitting to a Gaussian curve.
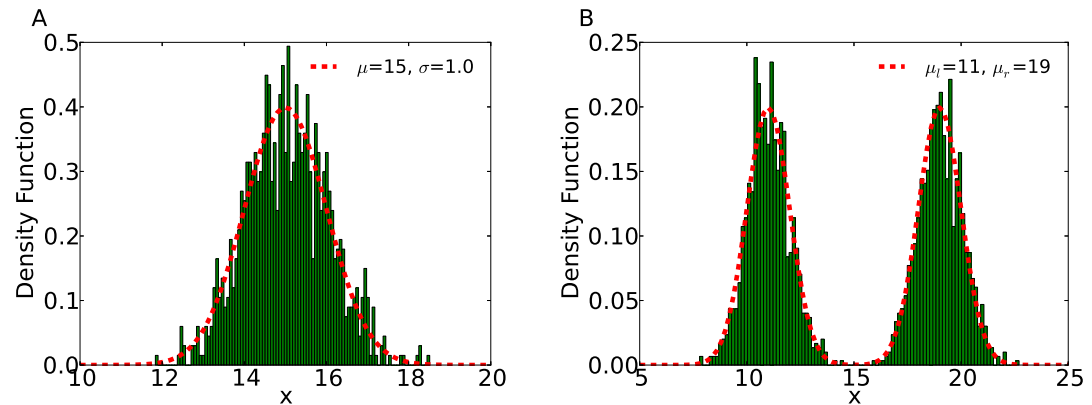
Figure 7. (A) Gaussian histogram distribution with $\mu = 15$ and $\sigma = 1.0$ and (B) bimodal histogram distribution of two Gaussian mixtures centered at $\mu_l = 11$ and $\mu_r = 19$.

Random Network Types

Several randomization procedures have been followed for this study (see Figure 8), but only the results based on R_{ER} have been published. The κ of all random graphs has been fixed to the network density of the brain graph based on the empirical AC map at each binarization level.

Double-edge swap (DES) method removes randomly chosen edges between node pairs *u-v* and *x-l* and creates new edges *u-x* and *v-y* which keeps the node degrees fixed (Hagberg et al., 2008).

Configuration model (CM) generates a random graph with a given degree sequence. The direct implementation of this model is to assign edges to the nodes randomly until the desired degree sequence is matched. The resulting random graph is expected to be a node-index-shuffled version of the original graph. However, these algorithms are non-trivial due to the occurrence of self-loops, when a node is connected to itself, and parallel edges, that is, multiple edges connecting two nodes (Newman, 2003; Hagberg et al., 2008). In this study, we used configuration model by checking parallel edge and self-loop occurrences, and applying the algorithm repeatedly, if they were the case.

Preserved degree distribution (PDD) tool searches for rewirable edge pairs for a user defined fraction of rewiring (rather than trying to rewire edge pairs at random) and generates a graph with the same degree distribution as in the input adjacency matrix (Rubinov and Sporns, 2010).

Partial randomization method takes adjacency matrices **A** and **B** and attempts to randomize matrix **A** by performing user defined number of rewirings, the rewirings avoid any spots where matrix **B** is nonzero (Rubinov and Sporns, 2010). Here we used the AC map for matrix **A** and an empirical functional connectivity map for matrix **B**, which was obtained from *1000 Functional Connectome Project* website *http://www.nitric.org/* according to the procedure described in Vuksanović and Hövel (2014).

Automated Anatomical Labeling

Table 1 shows the Automated Anatomical Labeling (AAL) for the cortical and sub-cortical brain regions (Tzourio-Mazoyer et al., 2002). The brain is partitioned into $N = 90$ regions symmetrically. AAL regions with index $n = 1, 2, \ldots, 45$ lie on the right R hemisphere, whereas $n = 46, 47, \ldots, 90$ on the left L. The middle column of table describes the position of AAL regions anatomically in the cortex, and the last column corresponds to abbreviations.

Table 1. Anatomical Description of Brain Nodes

| Index R/L	Anatomical Description	Label
1/46	Precentral	PRE
2/47	Frontal Sup	F1
3/48	Frontal Sup Orb	F10
4/49	Frontal Mid	F2
5/50	Frontal Mid Orb	F20
6/51	Frontal Inf Oper	F30P
7/52	Frontal Inf Tri	F3T
8/53	Frontal Inf Orb	F30
9/54	Rolandic Oper	RO
10/55	Supp Motor Area	SMA
11/56	Olfactory	OC
12/57	Frontal Sup Medial	F1M
13/58	Frontal Mid Orb	SMG
14/59	Gyrus Rectus	GR
15/60	Insula	IN
16/61	Cingulum Ant	ACIN
17/62	Cingulum Mid	MCIN
18/63	Cingulum Post	PCIN
19/64	Hippocampus	HIP
20/65	ParaHippocampal	PHIP
21/66	Amygdala	AMYG
22/67	Calcarine	V1
23/68	Cuneus	Q
24/69	Lingual	LING
25/70	Occipital Sup	O1
26/71	Occipital Mid	O2
27/72	Occipital Inf	O3
28/73	Fusiform	FUSI
29/74	Postcentral	POST
30/75	Parietal Sup	P1
31/76	Parietal Inf	P2
32/77	Supra Marginal Gyrus	SMG
33/78	Angular	AG
34/79	Precuneus	PQ
35/80	Paracentral Lobule	PCL
36/81	Caudate	CAM
37/82	Putamen	PUT
38/83	Pallidum	PAL
39/84	Thalamus	THA
40/85	Heschi	HES
41/86	Temporal Sup	T1
42/87	Temporal Pole sup	T1P
43/88	Temporal Mid	T2
44/89	Temporal Pole Mid	T2P
45/90	Temporal Inf	T3
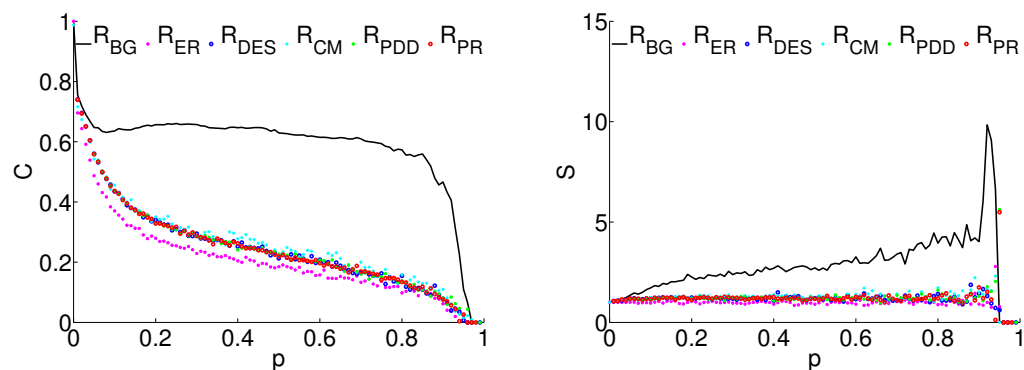
Figure 8. *C*- and *S*-values of brain graph R_{BG} and random graphs generated with different methods. Abbreviations stand for the resulting graphs from several randomization methods used: Erdős-Rényi-type R_{ER}, double-edge-swap method R_{DES}, configuration model R_{CM}, preserved degree distribution model R_{PDD}, partial randomization tool P_{PR}. The *S*-value is always calculated with respect to a corresponding Erdős-Rényi graph.